International Journal of Coal Science & Technology (2024) 11:13
https://doi.org/10.1007/s40789-024-00667-z

RESEARCH

Experimental and numerical simulation study on forced ventilation and dust removal of coal mine heading surface

Haotian Zheng[1,2,3] · Bingyou Jiang[1,2,3] · Haoyu Wang[1,2,3] · Yuannan Zheng[1,2,3]

Received: 31 May 2023 / Revised: 23 October 2023 / Accepted: 24 January 2024

Abstract

In order to study the problems of unreasonable airflow distribution and serious dust pollution in a heading surface, an experimental platform for forced ventilation and dust removal was built based on the similar principles. Through the similar experiment and numerical simulation, the distribution of airflow field in the roadway and the spatial and temporal evolution of dust pollution under the conditions of forced ventilation were determined. The airflow field in the roadway can be divided into three zones: jet zone, vortex zone and reflux zone. The dust concentration gradually decreases from the head to the rear of the roadway. Under the forced ventilation conditions, there is a unilateral accumulation of dust, with higher dust concentrations away from the ducts. The position of the equipment has an interception effect on the dust. The maximum error between the test value and the simulation result is 12.9%, which verifies the accuracy of the experimental results. The research results can provide theoretical guidance for the application of dust removal technology in coal mine.

Keywords Heading surface · Forced ventilation · Airflow field · Dust pollution

1 Introduction

In recent years, the mechanization level of coal mining has been greatly improved, and the safe and efficient coal mining is becoming mature (Ji et al. 2023; Wang et al. 2020; Yu et al. 2023). However, high concentration dust, which affects the safety of coal mine production and threatens the occupational health of coal mine employees for a long time, is still very serious (Jiang et al. 2023; Moreno et al. 2019; Zheng et al. 2023b).

At present, in addition to individual protection measures, coal dust control measures are commonly used at home and abroad: coal seam water injection to reduce dust, spray dust removal, ventilation dust removal and so on (Nie et al. 2017; Yu et al. 2017; Ashish et al. 2022; Han et al. 2023; Zhou et al. 2023; Zhu et al. 2023). Coal seam water injection reduces dust from the source, but there are problems such as water injection difficulty and low dust reduction efficiency (Geng et al. 2017; Wang et al. 2023; zhang et al. 2022a, b, 2023; Zhou et al. 2022). Spray dust removal requires a large amount of water and is not suitable for mines where water is scarce, and is prone to environmental pollution and nozzle blockage (Hou et al. 2022; Peng et al. 2022; Xiong et al. 2021). Ventilation is currently one of the more effective ways to remove dust, and a lot of research has been carried out at home and abroad. Zhou et al. found that the ventilation method of long pressure short extraction with the outlet of pressure duct 5 m away from the working face had the best dust removal effect, and the dust concentration could be rapidly reduced to less than 6 mg/m^3 (Zhou et al. 2020). Chen et al. used fluent software to numerically simulate the ventilation and dust removal system of the excavation face of rock roadway, and concluded that the average dust removal rates under the conditions of installing the wall duct, installing the dust collector and installing both at the same time were 49.4%, 67.1% and 86.2%, respectively (Chen 2018). Kurnia used computational fluid dynamics to evaluate a variety of strategies to improve dust dispersion generated at the

✉ Bingyou Jiang
cumtjiangby@163.com

1 Key Laboratory of Industrial Dust Prevention and Control & Occupational Health and Safety, Ministry of Education, Anhui University of Science and Technology, Huainan 232001, China

2 Joint National-Local Engineering Research Centre for Safe and Precise Coal Mining, Anhui University of Science and Technology, Huainan 232001, China

3 School of Safety Science and Engineering, Anhui University of Science and Technology, Huainan 232001, China

Published online: 12 March 2024

coal face and to ensure a safe level of dust concentration in mine tunnels to ensure operator safety (Kurnia et al. 2014). Toraño used CFD model to study the dust characteristics of the two auxiliary ventilation systems and found that the model accurately predicted the airflow and dust characteristics of the working face and different roadway sections (Toraño et al. 2011).

To sum up, most scholars have used numerical simulations to study the ventilation and dust removal at a particular site coal and rock excavation workface, and relatively few studies have carried out experimental research to explore the laws. Most of the coal mine heading faces use forced ventilation. However, the wind speed of the outlet and the distance from the outlet to the excavation face have great influence on the dust removal effect of the forced ventilation, so it is very important to study the forced ventilation dust removal. In this paper, we take the 25212 heading surface of Hongliulin Mine as a prototype and conduct an experiment by building a simulation test platform for ventilation and dust removal of coal mine heading surface, while combining numerical simulation technology to study the laws of airflow field changes and the spatial and temporal evolution of dust pollution. The study can provide guidance for the determination of the optimal wind speed of the roadway and the optimal distance from the pressure duct to the heading face. It can also provide theoretical basis for the installation position and opening time of the cyclone ventilation device attached to the wall on the mine duct, the air curtain device on the tunneling machine, and the automatic purification water curtain.

2 Experimental and simulation method

2.1 Establishment of similar experimental platform

2.1.1 Design of experimental platform

The 25212 roadhead in the Hongliulin coal mine in Shaanxi Province is used as a prototype, the roadhead is approximately 4 m wide and high, and the roadhead is ventilated by a press-in type ventilation method. There are 2 sets of FBD No. 8.0/2 × 55 local ventilation fans (1 of which is standby), with motor power of 2 × 55 kW, air volume of 680–880 m^3/min, and noise of ≤ 85 dB. The press-in local ventilation fan is placed in the 25213 exiting frame lane, 30 m west of 25212 bypass. The maximum air supply distance is 3200 m. The press-in ducts are extended to the face of the working face through the 25213 outframe lane and the 25212 outframe lane. The anti-static soft wind pipe with a diameter of 1000 mm is used. The press-in ducts are arranged at the top of the right gang of the roadway, and are laid and hung according to the regulations. The maximum air volume of the working face is 412 m^3/min and the air volume of the roadway at the fan is 975 m^3/min. The site of heading face 25212 is shown in Fig. 1. The ventilation schematic diagram of the working face is shown in Fig. 2.

To ensure the feasibility of the test, the original dimensions were scaled using the similarity criterion to build the experimental platform, using the 25212 heading surface of the Hongliulin coal mine in Shaanxi Province as the prototype. The model was designed according to the reality: model = 2: 1, section height of the model was 2 m, width was 2 m, and length was 9 m. As the dust generated by the heading face tends to stabilize its distribution with the increase of movement distance, the length of the model roadway is not designed according to the actual type length. The distance from the outlet of the air duct to the working face is calculated according to the formula (1) of the effective range. The cross-sectional area of the roadway head is 4 m^2, so the distance from the outlet to the working face should be less than 3 m.

$$L_s \leq 1.5\sqrt{S} \tag{1}$$

where S is the cross-sectional area and L_s is the distance from the air outlet to the head.

The roadway adopts the pressure-in ventilation mode, and the turbine fan with the power of 15 kW provides variable frequency air supply. The pressure air duct is composed of an acrylic fixed air duct with a diameter of 0.4 m and a movable flexible air duct. The outlet is equipped with a bidirectional wind speed sensor for mining. The adjustable distance between the air outlet and the driving face is 1–3 m. The dust generation system of the device is composed of an aerosol generator, an air pump, a gas pipe and a moving mode group. The aerosol generator is located at the front end of the roadway and

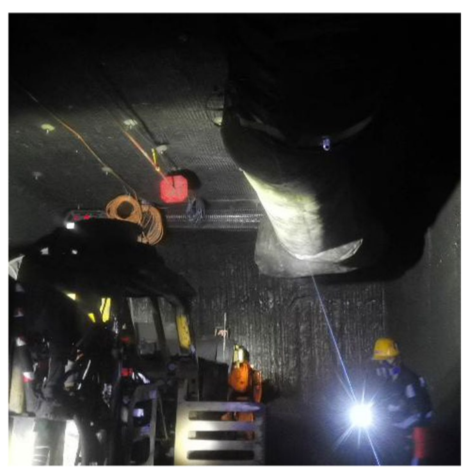

Fig. 1 Site of heading face 25212

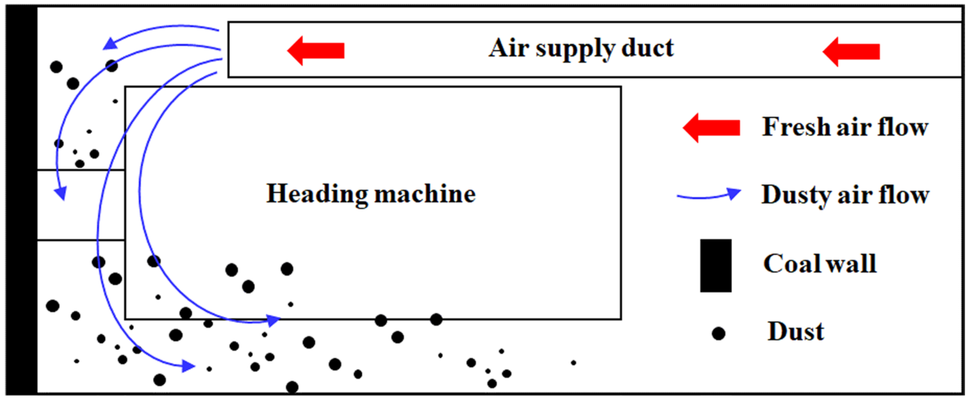

Fig. 2 Ventilation diagram of working face 25212

can move on the end face with a moving range of 0–1 m and a precision of 1 mm. Airflow speed, dust height, air duct distance from the head position and other parameters can be adjusted in real-time visual control console. Taking the central position of the end face where the aerosol generator is located as the coordinate origin, *X* direction indicates that the tunnel head points to the end of the tunnel, *Y* direction indicates that the tunnel pressure side points to the roadheader, and *Z* direction indicates that the tunnel floor points to the roof. The experimental model roadway is shown in Fig. 3.

2.1.2 Experimental method

2.1.2.1 Preparation of experimental materials The coal sample used in the experiment was taken from Hongliulin Mine in Shaanxi Province, and the fresh lumps of coal were taken out from under the mine, sealed with cling film and brought to the laboratory. The coal briquettes were put into a planetary ball mill for grinding, which was operated at a frequency of 50 Hz and the running time is 1 h. To ensure uniform dust emission from the dust collector, the coal powder was put into a drying box at 40 °C for 24 h before the experiment. Finally, 0.2 g of coal powder was taken and the dust particle size was determined by Malvern particle size analyser. The particle size of the dust can be set as a CFD

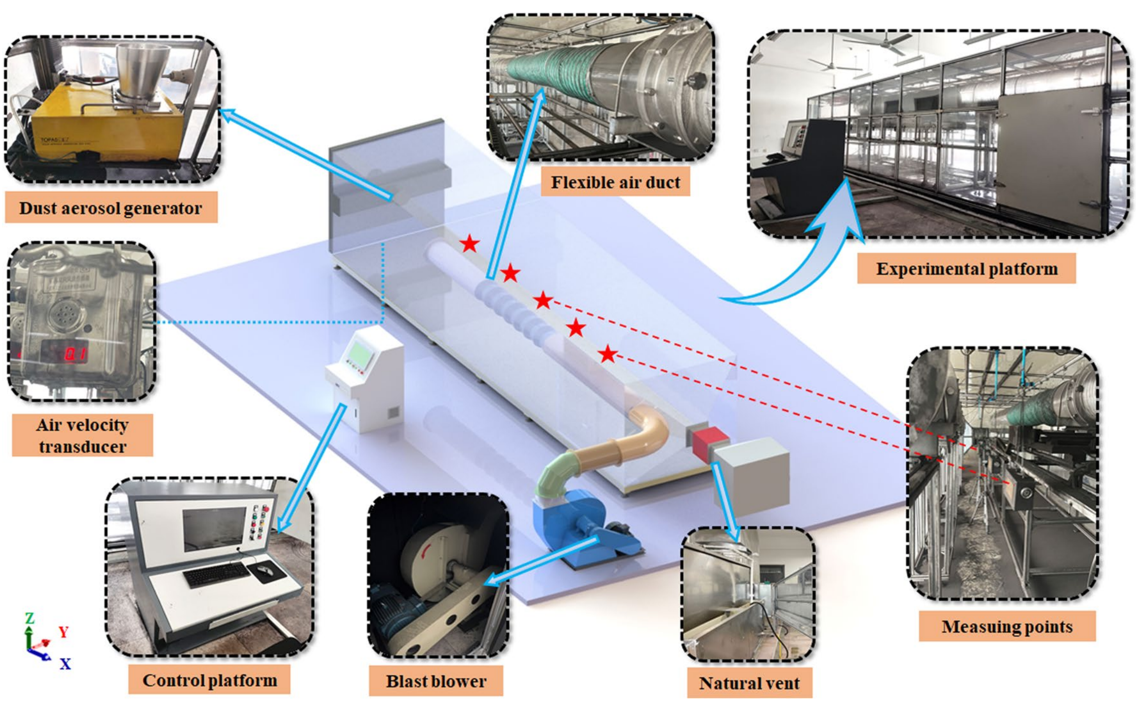

Fig. 3 Simulation test platform for ventilation and dust removal of heading surface

Table 1 The characteristic particle size of coal dust

Item	Characteristic particle size (μm)		
	D10	D50	D90
Value	13.370	53.680	123.078

parameter, with a minimum dust diameter of 1 μm and a maximum dust diameter of 200 μm. The characteristic particle size of coal dust sample is shown in Table 1. The particle size distribution curve is shown in Fig. 4. The fitting result of Rosin–Rammler function is shown in Fig. 5.

The instrument for measuring dust mass concentration is CCZ-20A dust sampler (Jiangsu Changshu Yushan Company), with sampling flow of 20 L/min and working noise ≤ 75 dB(A). Polypropylene fiber filter membrane (Shandong Weifang Jukai electronic technology company) is selected for dust collection, with specifications of 40 mm and aperture of 0.8 μm.

2.1.2.2 Pressure ventilation parameters setting There are many factors affecting dust concentration of roadway under forced ventilation, among which the most important ones are wind speed of outlet and distance from outlet to driving

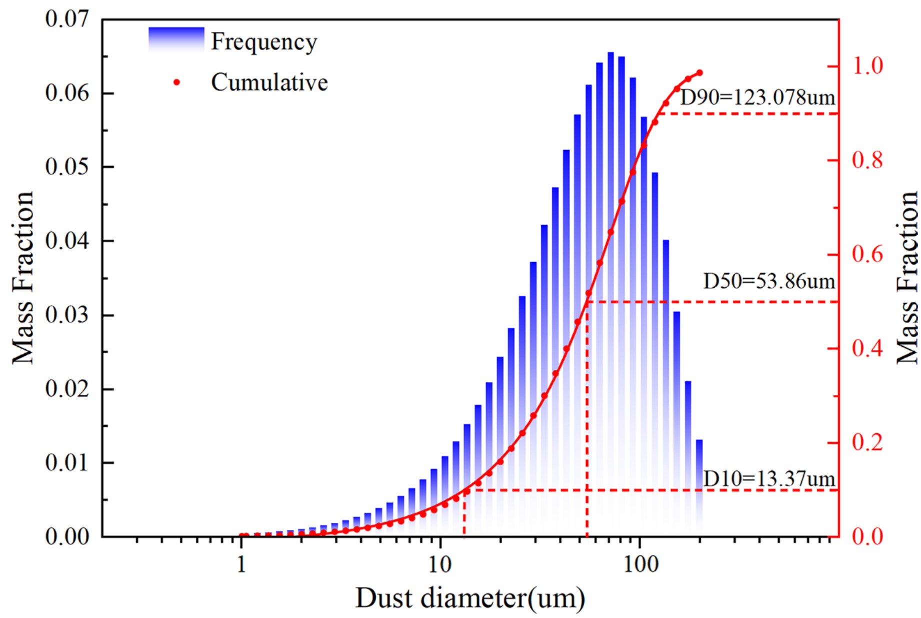

Fig. 4 Particle size distribution curve of dust

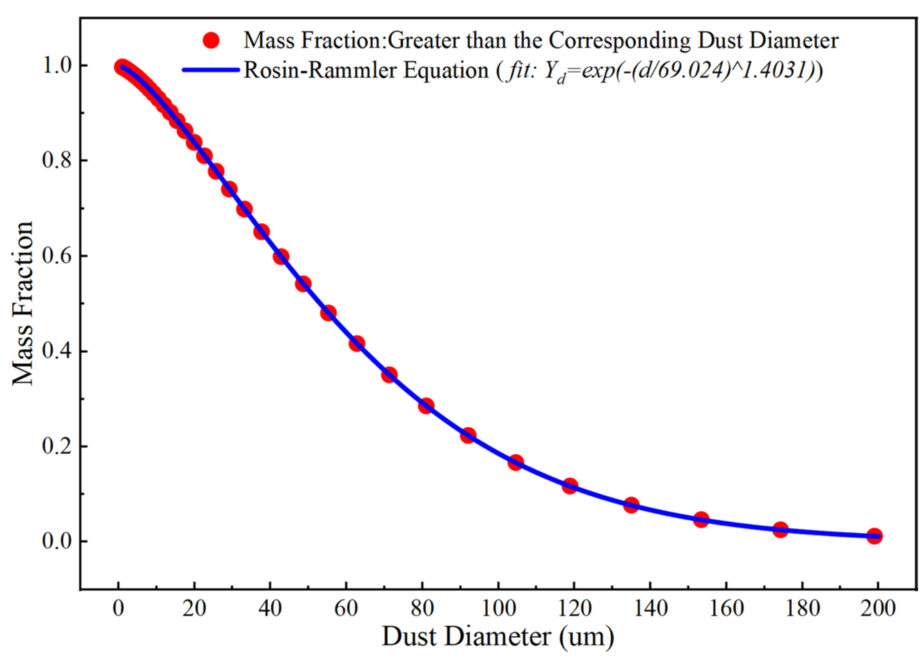

Fig. 5 Fitting result of Rosin–Rammler function

face (Hua et al. 2018). In this paper, the control variable method was used to study the changes of dust mass concentration with different wind speed and different distance from the pressure duct to the head. Firstly, the distance from the pressure air outlet to the head is kept at 2 m, and the air speed is set at 0.5, 1.0, 2.0, 3.0 and 4.0 m/s respectively for the dust mass concentration, and the optimal air speed is selected. Then, under the optimal wind speed, the dust mass concentration of 1.0, 1.5, 2.0 and 2.5 m from the pressure duct to the driving face was studied. The measuring points were arranged at 1, 2, 3, 4 and 5 m from the head, and the height of the measuring points was kept at 0.75 m above the human breathing zone.

2.1.2.3 Measurement of dust mass concentration The experimental installation uses a TOPAS brand dust generator (SAG410) manufactured in Germany. To ensure the uniform and stable dust generation from the aerosol generator, the coal dust is dried before each experiment. The operating power of the dust generator is controlled by the air flow. The power of the dust generator is maintained at 20% and the dust generation rate is maintained at 1000 mg/s. The pressure air duct of the roadway is kept ventilated, and the operating platform is used to control the wind speed, the height of the aerosol generator and the distance between the outlet and the driving face. The dust mass concentration at each measuring point was measured by CCZ-20A dust sampler. In order to reduce the random error of the test, the filter film was put into a drying box at 100 ℃ for 30 min before and after weighing. The filter film before and after the test was weighed by an electronic balance, and the dust mass concentration at each measuring point was calculated by Eq. (2). Each weighing was repeated 3 times and averaged. Figure 6 shows the specific procedure.

$$C = \frac{m_2 - m_1}{Q \times t} \times 1000 \tag{2}$$

where, C is the dust concentration at measuring point, mg/m^3; m_2 is the mass of the sampled membrane, mg; m_1 is the mass of the filter membrane before sampling, mg; Q is the sampling flow, L/min; t is the sampling time, min.

2.2 Building of CFD model

The diffusion and diffusion process of dust in heading face under the action of air flow belongs to the category of gas–solid two-phase flow. Eulerian-Lagrange method was used to calculate and solve the process. Euler method focuses on the physical quantity change of particles at every point and moment in space, regardless of the motion of individual particles. Therefore, the flow is regarded and described as a continuous phase in the Euler coordinate system. Lagrange method focuses on the study of each particle, describing the motion process of particles at any time and the change of physical quantity over time. Thus, dust particles are treated as discrete phases and described in Lagrangian coordinates (Jin et al. 2022; Liu et al. 2019; Nie et al. 2022b). The following assumptions are made for the model:

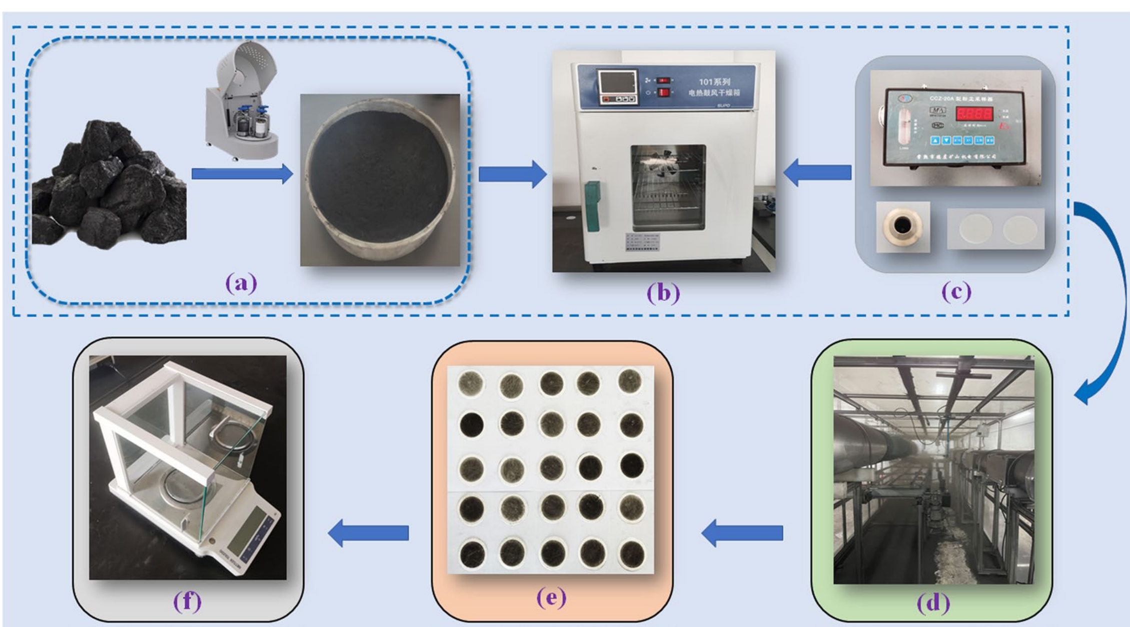

Fig. 6 Diagram of the experimental process. **a** Pulverized coal preparation **b** Drying of pulverised coal and filter membranes **c** Dust sampler selection **d** Alleyway testing **e** Collection of filter membranes **f** Measurement of dust concentration

(1) Air flow is an incompressible fluid.
(2) The interaction between particles and the influence of particles on the continuous phase are ignored.
(3) All dust is seen as a sphere.
(4) Energy exchange is not considered.

Dust is subjected to multiple forces during its movement (Chhabra 2019). According to Newton's second law, the force balance equation of dust is

$$\frac{d\vec{u}_{\mathrm{p}}}{dt} = \frac{\vec{u} - \vec{u}_{\mathrm{p}}}{\tau_r} + \frac{\vec{g}\left(\rho_{\mathrm{p}} - \rho\right)}{\rho_{\mathrm{p}}} + \vec{F} \tag{3}$$

where $\frac{\vec{g}(\rho_{\mathrm{p}}-\rho)}{\rho_{\mathrm{p}}}$ is gravity, $\vec{F}$ is the additional force, $\frac{\vec{u}-\vec{u}_{\mathrm{p}}}{\tau_r}$ is the drag force of the unit particle, and

$$\tau_r = \frac{\rho_{\mathrm{p}} d_{\mathrm{p}}^2}{18\mu} \frac{24}{C_{\mathrm{d}}\mathrm{Re}} \tag{4}$$

where τ_r is the particle relaxation time, u is the airflow velocity, u_{p} is the dust particle velocity, μ is the airflow viscosity, ρ is the airflow density, ρ_{p} is the dust particle density, and d_{p} is the dust particle diameter. Re is the relative Reynolds number, defined as

$$\mathrm{Re} = \frac{\rho d_{\mathrm{p}}\left|\vec{u}_{\mathrm{p}} - \vec{u}\right|}{\mu} \tag{5}$$

The additional forces $\vec{F}$ include the "virtual mass" force, pressure gradient force, thermophoretic force, etc. Based on previously published research on dust particles (V.K. Kollipara 2015), this paper does not consider the existence of additional forces.

2.2.1 Establishment of physical model

In order to realize the numerical simulation to reflect the effect of the test situation, this paper takes the test roadway as the prototype, simplifies the prototype to a certain extent, and uses Solidworks software to establish the physical model of the test roadway at 1: 1, the model size is 2 m×2 m×9 m. Since dust is generated from the roadway head in the driving process, the roadway head in the model is set as the dust emission surface. The parameters used are listed in Table 2, and the physical model and grid of the test roadway are shown in Fig. 7.

2.2.2 Grid independence test

When computational fluid dynamics is used to simulate airflow field and dust diffusion, the quality of the grid will directly affect the efficiency and accuracy of the simulation, so it is necessary to verify the grid independence of the physical model. Air flow is the main factor restricting dust diffusion law and dust pollution effect. Therefore, wind speed distribution along the normal central axis of the roadway at the height of human respiratory tract is selected as the grid independence verification parameter. ICEM software was used to divide the physical model into unstructured grids, and three different numbers of grids (Scheme 1, Scheme 2, Scheme 3) with coarse (324, 185 units), medium (817, 508 units) and fine (3, 044, 823 units) were generated. The quality of the grids was all greater than 0.3. As can be seen from Fig. 8, the wind speed reaches the maximum at 0.08 m of the heading face, and the wind speed is 0.97 m/s (coarse grid), 0.71 m/s (medium grid), and 0.66 m/s (fine grid) respectively. The wind speed reaches the lowest at 0.315 m from the heading face, and the wind speed is 0.37 m/s (coarse grid), 0.14 m /s (medium grid) and 0.10 m/s (fine grid) respectively. The wind speed at 0.3 m to 1.3 m from the heading face fluctuates constantly, which may be due to the influence of equipment storage in the roadway, where there is eddy current and the wind speed is relatively chaotic. After 2.76 m from the heading face, the wind speed showed a decreasing trend. In contrast, the velocity values of coarse grid and fine grid have the largest deviation, and the trend of wind velocity curves of medium grid and fine grid is roughly the same. For example, compared to a fine grid, at the peak of the velocity curve, the relative error of the coarse grid is 31.9%, while the error of the medium grid is only 7.5%. At the valley of the velocity curve, the relative error of the coarse grid is 31.4%, and the error of the medium grid is only 0.3%. Considering the computer performance and computational efficiency, we selected a medium grids to carry out follow-up research.

Table 2 Geometrical parameters used in the present model

Properties	Value (m)
Length of the roadway	9
Height of the heading face	2
Width of the heading face	2
Diameter of air duct	0.4
Distance from duct to face	1–3
Size of the roadheader	3×1.3×1

2.2.3 Boundary conditions and parameter setting

The grid file was imported into Fluent, and the model boundary and dust parameters in the model tree of the software interface were set according to the specific conditions of the 25212 heading face, as shown in Table 3.

The calculation flow chart includes preprocessing, solve and post-processing, as shown in Fig. 9.

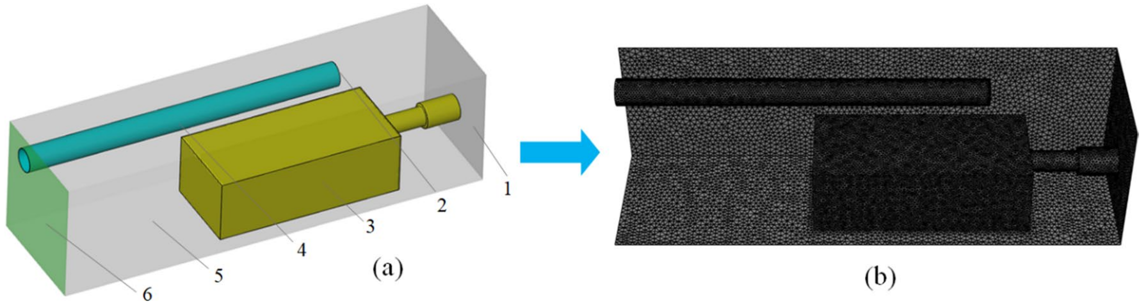

Fig. 7 Experimental roadway. **a** Physical model. 1-Heading face; 2-Airflow inlet; 3-Roadheader; 4-Roadway; 5-Air duct; 6-Outlet. **b** Grid model

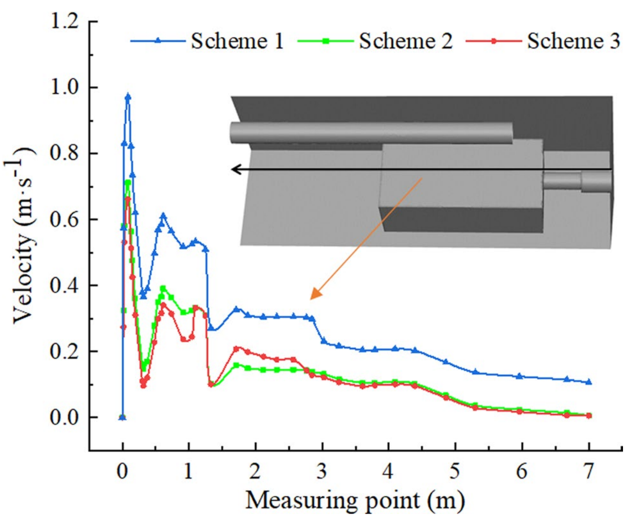

Fig. 8 Changes of wind speed along different grid conditions

Table 3 Simulation parameters used in the present model

Name	Property	Value and parameters
General	Solver type	Pressure-based
	Gravity	9.81 m/s^2
	Time	Transient
Viscous model	k-epsilon	Standard wall treatment
Material (Air)	Density	1.225 kg/m^3
	Viscosity	1.79×10^{-5} kg/(m s)
	Velocity magnitude	20 m/s
Inlet	Turbulent intensity	3.07%
	Hydraulic diameter	1 m
Outlet	Type	Outflow
	Method	SIMPLE
Solution	Initialization method	Standard
	Injection type	Surface
	Material	Coal-hv
	Diameter distribution	Rison-rammler
Discrete phase	Min. diameter	1×10^{-6} m
	Max. diameter	2×10^{-4} m
	Mean diameter	6.9×10^{-5} m
	Spread parameter	1.4
	Number of diameters	10
	Drag law	Spherical

3 Analysis of ventilation and dust removal test and simulation results

3.1 Analysis of test results of pressure ventilation dust removal

3.1.1 Variation of dust mass concentration with wind speed

In this paper, the experimental results are fitted using Origin 2023. The variation law of dust concentration with wind speed is shown in Fig. 10. The higher the wind speed, the faster the dust concentration decreases. The dust mass concentration in the roadway decreases gradually from the head to the rear side of the roadway. When $L < 1.4$ m, the dust mass concentration gradually decreases with the increase of wind speed, indicating that when the wind speed is low, the driving effect of air flow is not enough to effectively discharge dust from the roadway, and the dust concentration may gradually accumulate. When the wind speed increases, the pushing effect of the air flow is strengthened, which can carry away the dust more effectively, so that the dust concentration is gradually reduced. When $L > 1.4$ m, when the wind speed in the roadway is too high, the mass concentration of dust at each measuring point increases, indicating that when the pressure duct is a certain distance from the driving face, the greater the wind speed, the dust accumulated on the ground may be raised again, resulting in the phenomenon of rising dust concentration in the roadway. When the distance between the pressure tuyere and the driving face is 1.8 m, the dust mass concentration is the lowest when the wind speed is 2 m/s, about 30 mg/m^3. When the distance between the air pressure tuyere and the driving face is 2.2 m, the dust

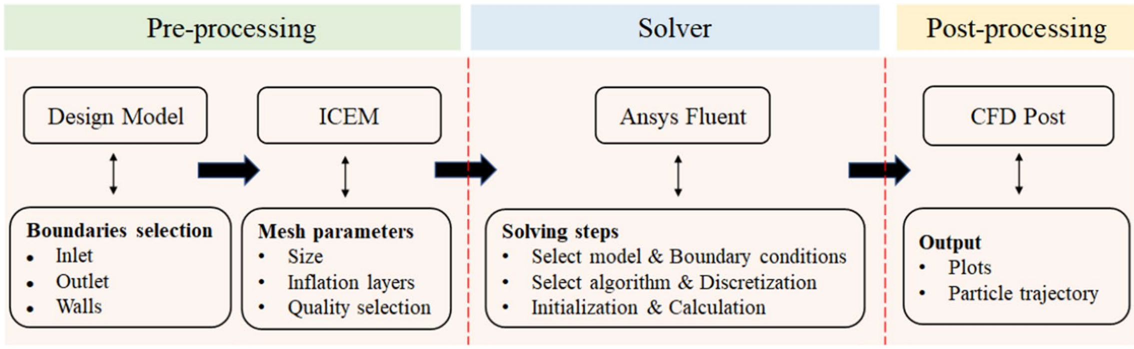

Fig. 9 Flow chart of calculation process

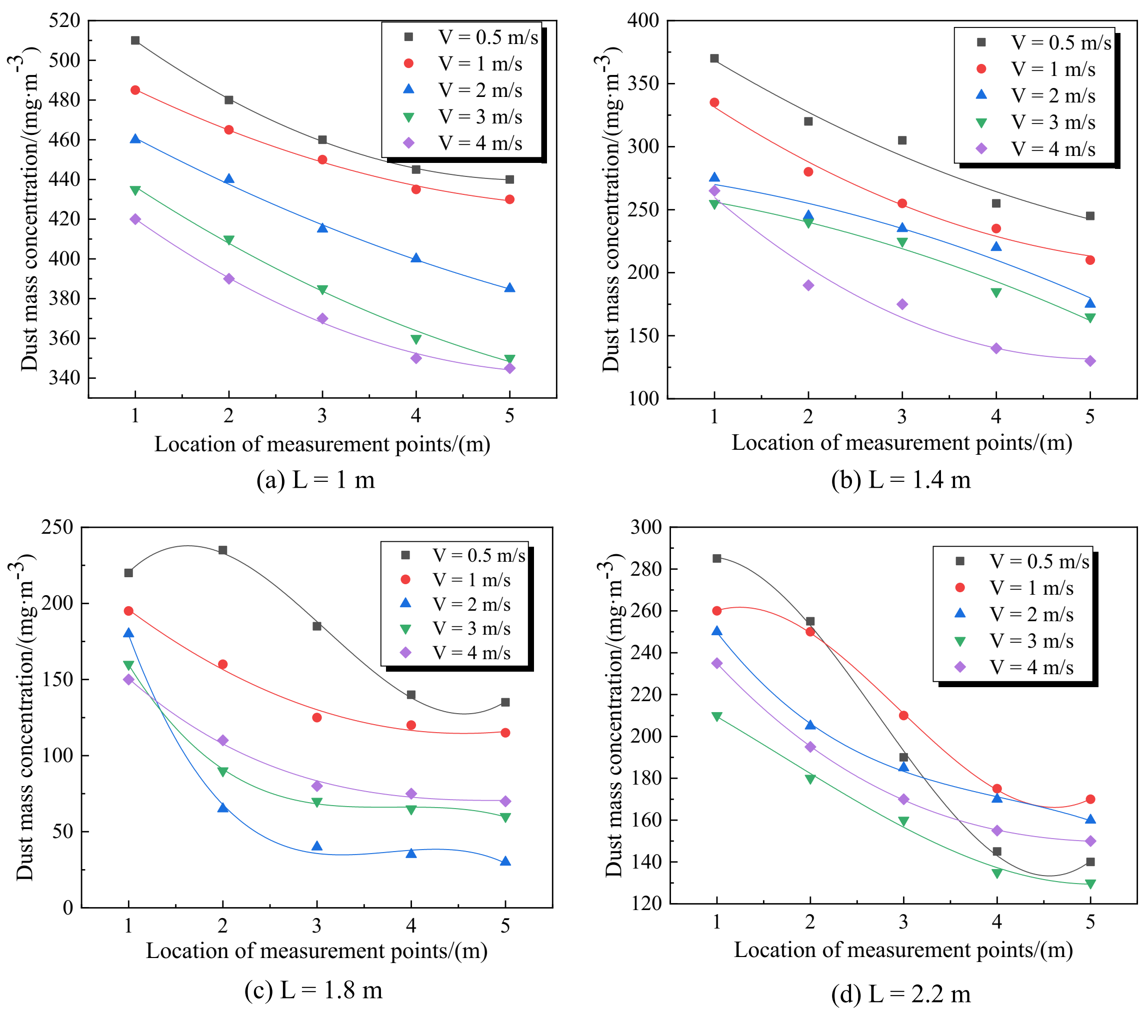

Fig. 10 Dust mass concentration at different wind speeds. **a** $L=1$ m **b** $L=1.4$ m **c** $L=1.8$ m **d** $L=2.2$ m

mass concentration is the lowest when the wind speed is 3 m/s, and the lowest concentration is 130 mg/m^3. It shown that the increase of wind speed in the compressed ventilation tunnel is not unlimited, and the high wind speed may bring about some negative effects, such as excessive airflow resistance and increased energy consumption. In order to achieve the best dust removal effect and energy consumption balance, the wind speed of the forced ventilation system should be controlled within a suitable range. Therefore, from the perspective of minimum dust concentration and energy saving, when the wind speed is 2 m/s and the distance between the pressure tuyere and the driving face is 1.8 m, the dust concentration in the roadway is minimum, and the parameter setting of the roadway is reasonable.

3.1.2 The variation of dust mass concentration with distance

The measurement results of dust mass concentration with distance were nonlinear fitted, as shown in Fig. 11. When the distance from the air outlet to the heading surface is 1 m, the dust mass concentration is the highest, up to 510 mg/m^3, indicating that when the pressure air outlet is too close to the heading face, dust tends to accumulate in the roadway and the ventilation and dust removal effect is poor. First of all, the limited time and space for fresh air to enter the heading face will limit the coverage of the airflow, making it impossible for dust to be effectively carried away from the vicinity of the digging face, thus affecting the dust control effect. Secondly, the close proximity leads to disturbed airflow and the close air supply may result in direct contact between the airflow and the surfaces of equipment and tools on the digging face, thus creating turbulence or backflow prematurely.

The dust concentration decreases significantly with increasing distance from the pressure air outlet to the digging face, and the further the distance, the lower the dust concentration. However, when the distance between the air outlet and the heading face is 1.8 m, the dust mass concentration is the minimum, and when the distance between the air outlet and the heading face is 2.2 m, the dust mass concentration increases again, because when the distance between the air outlet and the heading face is too far, the fresh air may be subject to some resistance during the transmission process, resulting in a slower airflow, and the reduction of air volume makes it insufficient to dilute the dust mass concentration, resulting in an increase of dust in the air. When the distance between the pressure duct and the driving face is close, the fresh air can reach the driving face quickly and form a strong airflow. In this situation, the air supply effect of the pressure duct is good, and the dust can be effectively taken away from the vicinity of the driving face, thus reducing the dust concentration. Therefore, the reasonable choice of the distance between the outlet and the heading face is very important to the influence of the change of roadway dust concentration. In summary, there are optimal values for both wind speed and distance from the air outlet to the headway. Considering the lowest dust

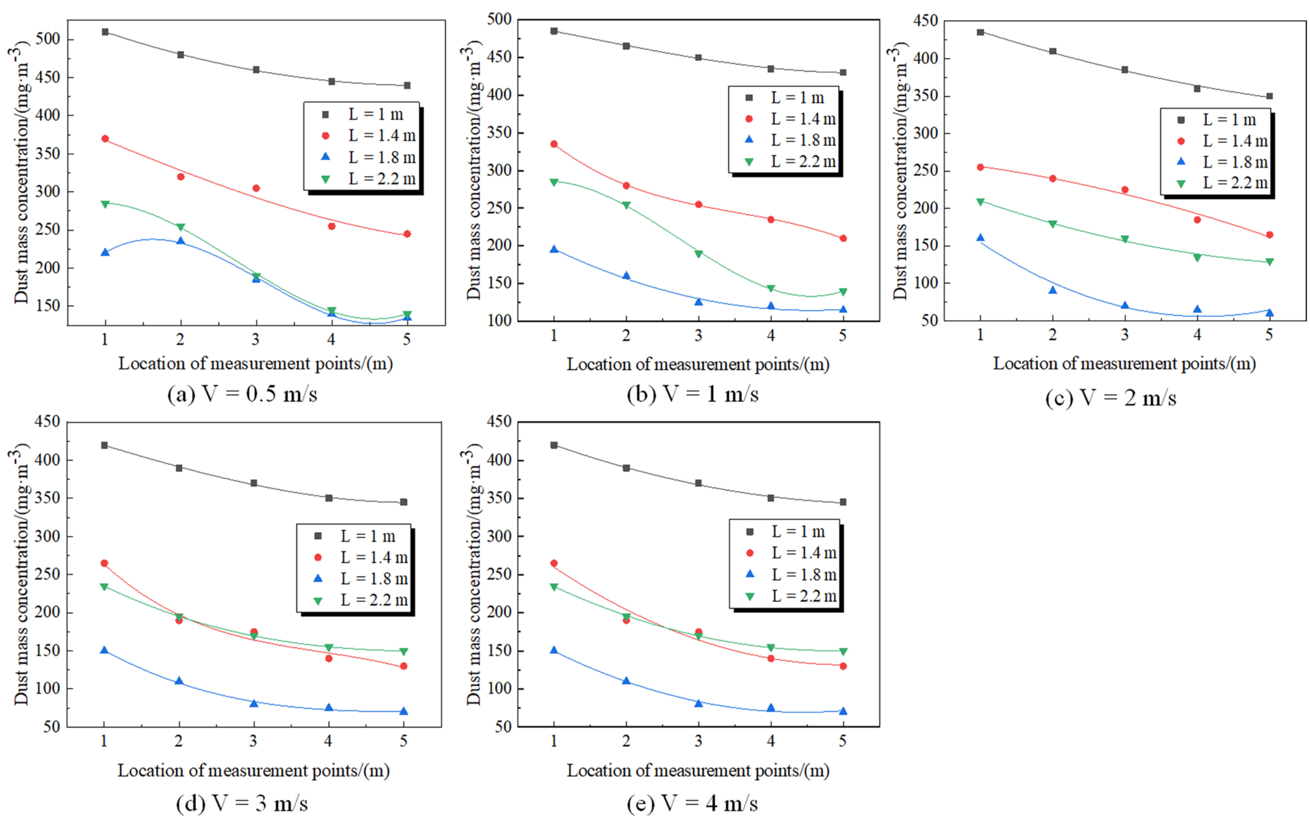

Fig. 11 Dust mass concentration at different distance from pressure duct to heading surface. **a** $V=0.5$ m/s **b** $V=1$ m/s **c** $V=2$ m/s **d** $V=3$ m/s **e** $V=4$ m/s

concentration in the roadway and energy saving, when the wind speed is 2 m/s and the distance from the air outlet to the heading surface is 1.8 m, the dust concentration in the roadway is the lowest and the roadway parameter setting is reasonable.

3.2 Analysis of test results of pressure ventilation dust removal

From Sect. 3.1, it is concluded that the dust mass concentration in the roadway is minimum when the wind speed is 2 m/s and the distance from the air outlet to the headway is 1.8 m. Therefore, the author used ANSYS-Fluent software to simulate the change of wind flow field and the spatial and temporal evolution of dust pollution under this optimal working condition, and compared them with the experimental results. The experimental and numerical simulation results are shown in Fig. 12, with a minimum error of 6.5% and a maximum error of 12.9% at each measurement point. This shows the correctness and validity of the numerical simulation results, which can be further analysed.

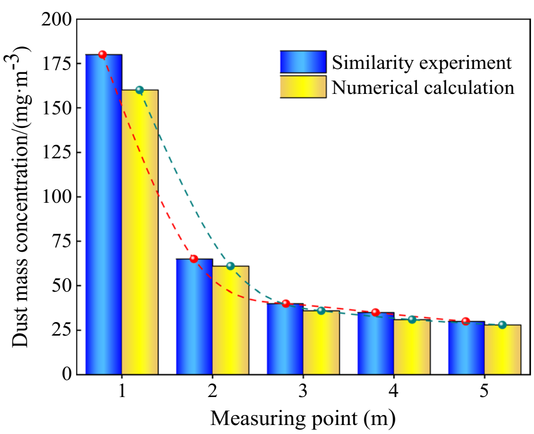

Fig. 12 Comparison of dust mass concentration between experimental and numerical simulation under optimal working conditions

3.2.1 Variation law of airflow field

The distribution of the wind flow field in the roadway with and without the influence of dust is shown in Fig. 13. The airflow field in the roadway can be divided into three areas: the jet zone, the vortex zone and the reflux zone (Nie et al. 2022a). The jet zone is the area where the air flows from the outlet of the duct to the heading face, the air velocity in this area is very high, in the shape of a jet, and has strong characteristics of straight-line movement, which is recorded as zone I. Due to the restriction of the confined space of the roadway and the influence of the continuity of the wind flow, the flow in the opposite direction of the jet soon appears, and the wind flow forms a backflow area in the working area, which is recorded as zone II. At the same time, due to the suction of the jet, there is also a vortex zone at the interface between the jet and the return zone, which usually has a lower flow velocity and a rotational, spiral or cyclonic motion of the air flow, which is recorded as zone III. The interaction between the dust field and the airflow field is due

Fig. 13 Distribution of airflow field in roadway. **a** Dust-free air flow field **b** Air flow field with dust

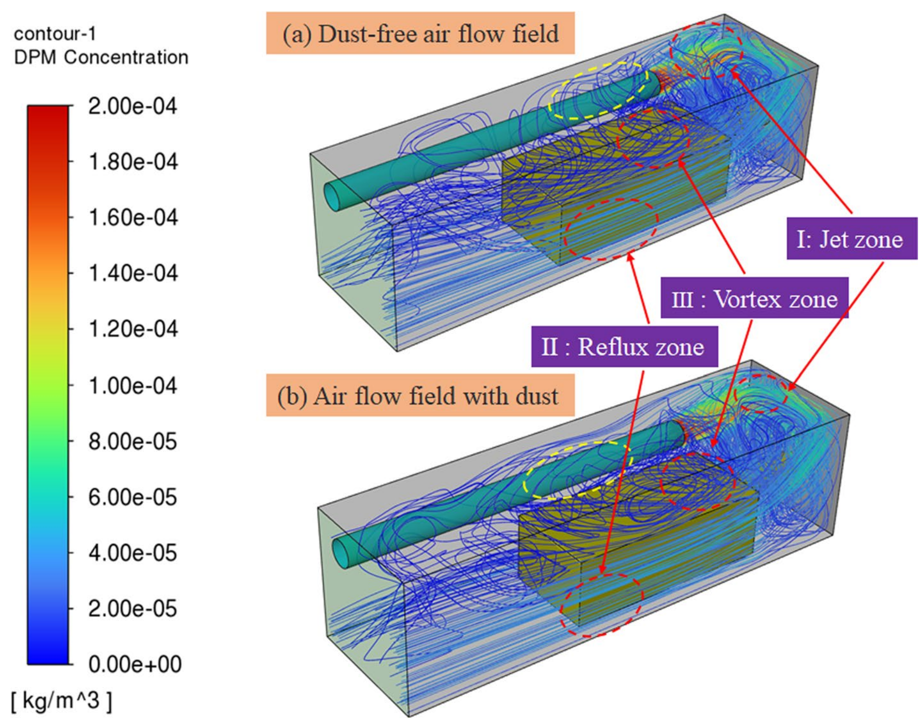

to the fact that when there is a large amount of dust in the air, the dust particles interact with the airflow, slowing it down and changing the direction and distribution of the airflow, thus affecting the flow properties and transfer characteristics of the airflow. Specifically in the wind flow distribution near the location of the wind cylinder is different, with the dust impact of the wind flow field here is a vortex, no dust impact is a backflow.

The formation of the jet, return and vortex zones in the wind flow field takes a certain amount of time and depends on various factors such as air velocity and environmental conditions. The spatial and temporal evolution of the wind flow field in the tunnel is shown in Fig. 14. When the wind speed is 2 m/s and the distance from the air outlet to the heading face is 1.8 m, the jet zone and the reflux area on the side away from the wind pipe are formed at about 10 s, but at this time the airflow distribution in the roadway is still relatively disorderly, after a period of evolution, the return flow area on the side of the pressure duct is formed at about 40 s, and a more obvious jet zone and return flow area are gradually formed in the tunnel at about 50 s, but the vortex area is not yet obvious, and when it reaches at 60 s the three zones become more obvious and stable. Higher air velocities can facilitate the formation of jet zones, while slower airflows may take longer to form jet zones. The surrounding environment also has an impact on the formation of jet, vortex and reflux zones (Yin et al. 2020). Obstructions, flow boundaries or other airflow disturbances in the environment may prevent the formation of jet zones and take longer to achieve stability.

As L increases, turbulence effects generally become more significant. The turbulence energy contour is shown in Fig. 15. The velocity vector diagram at the height of the human breathing zone is shown in Fig. 16. The contour of dust mass concentration at the height of human breathing zone is shown in Fig. 17. The contour plot shows the variation of turbulent energy at different locations, with regions with higher energy usually corresponding to regions with

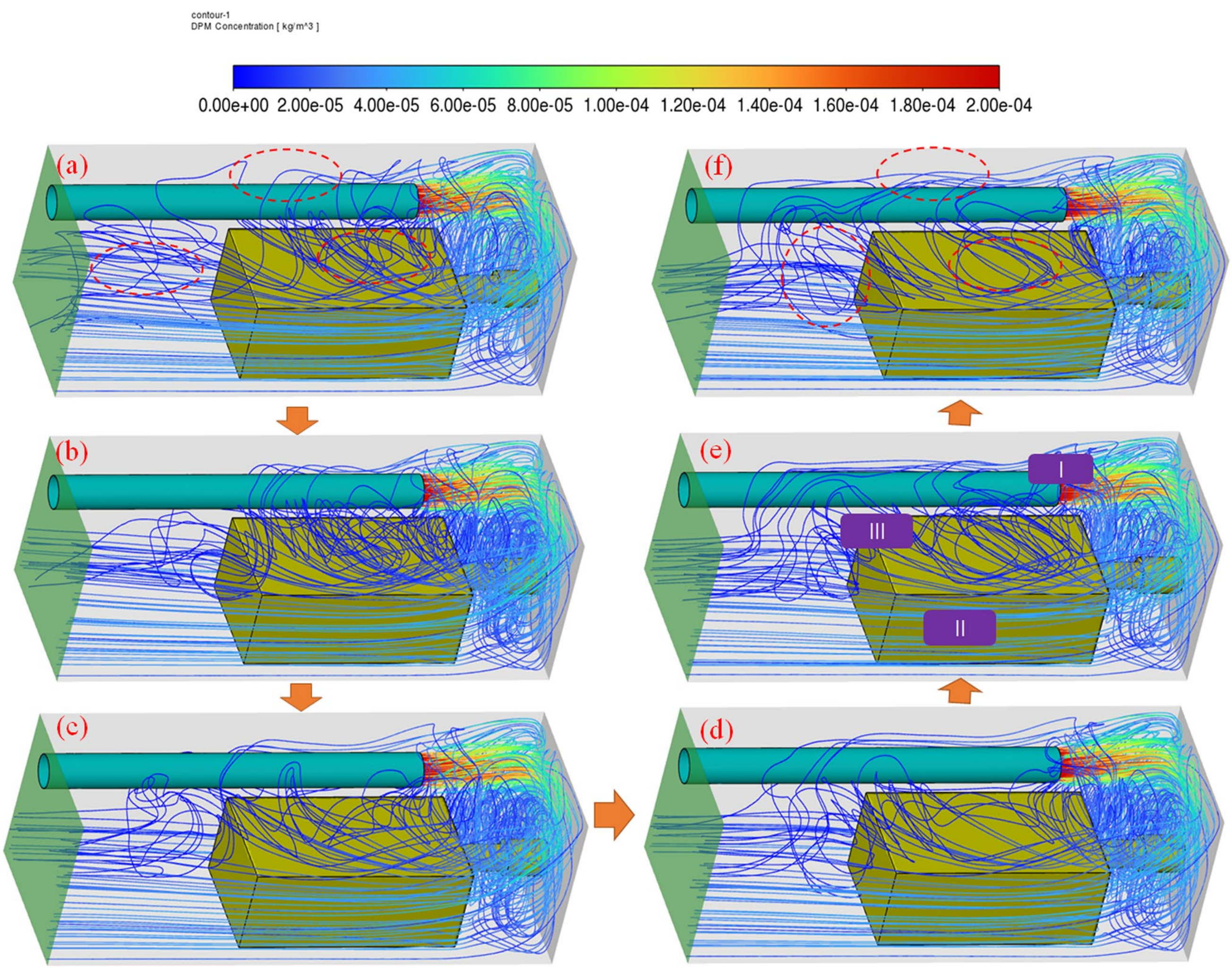

Fig. 14 The spatial and temporal evolution of the airflow field in the roadway. **a** $t=10$ s **b** $t=20$ s **c** $t=30$ s **d** $t=40$ s **e** $t=50$ s **f** $t=60$ s

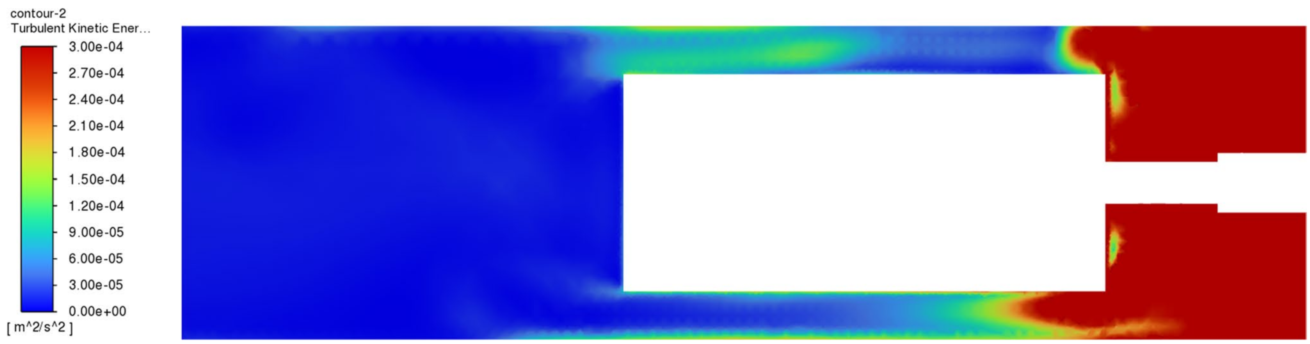

Fig. 15 Turbulence contour at the height of human breathing zone

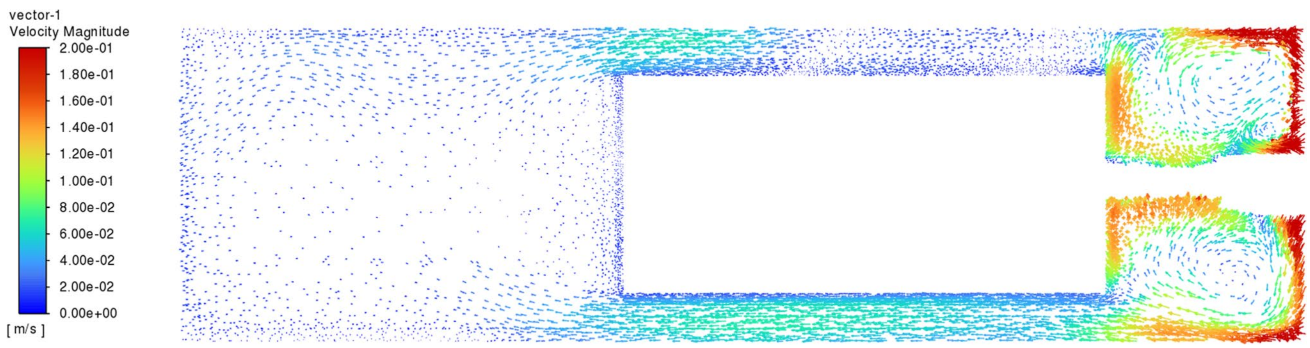

Fig. 16 Velocity vector diagram at the height of the human breathing zone

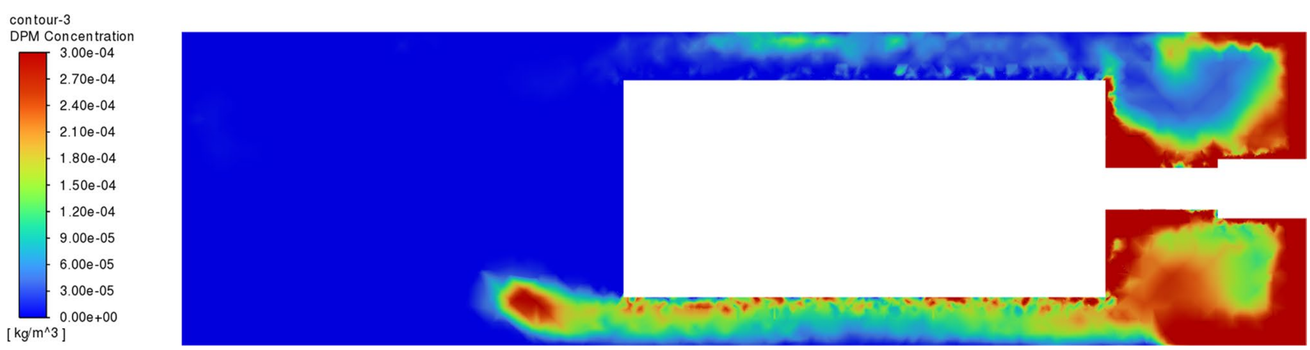

Fig. 17 Contour line of dust mass concentration at the height of human breathing zone

stronger turbulence. If dust particles are present in these high-energy regions, they may be affected by turbulence and accumulate, resulting in unusually high dust concentrations. It can be seen from the contour line that there are two eddy currents at the front end of the heading machine, and the dust mass concentration in the roadway basically decreases gradually from the head of the roadway to the back side of the roadway. The dust mass concentration on the side away from the pressure duct is significantly higher than that on the other side.

3.2.2 Spatial and temporal model of dust pollution

The diffusion of dust concentration in the roadway over time is shown in Fig. 18. When the wind speed is low, the dust diffusion is slow and mainly concentrated at the front end. As time passes, the dust gradually diffused to the rear side of the roadheader, and the dust concentration on the rear side of the roadway gradually increased and reached stability at 60 s. This phenomenon shows that the diffusion of the dust field is usually shown as the formation of a concentration

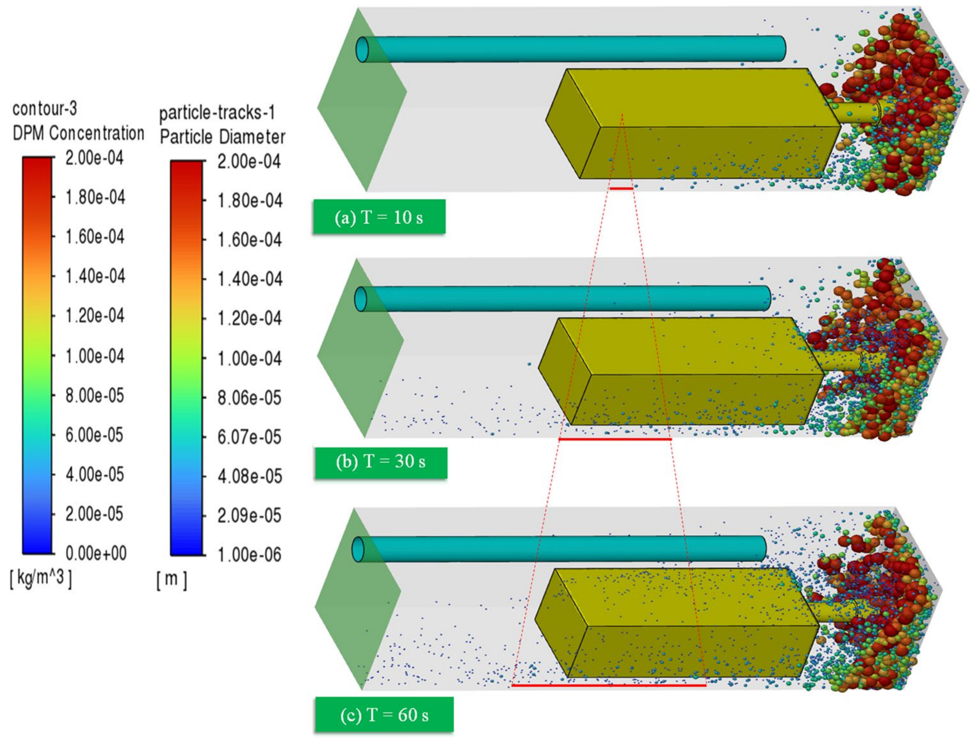

Fig. 18 Dust diffusion in roadway at different time. **a** $T=10$ s **b** $T=30$ s **c** $T=60$ s

gradient, with dust particles spreading from the initial release point to the surrounding area, forming a gradient of decreasing concentration. The reason may be that the size of different particles influences the diffusion behavior. Larger particles usually settling over short distances, while smaller particles can be diffused over longer distances by the airflow. In addition, the air flow can affect the suspension, transportation and settling of dust particles in the roadway. The turbulence effect in the environment can increase the mixing degree between particles and air flow, promote the agglomeration of dust particles and the diffusion of dust particles to the rear of the tunneling machine.

According to the changes of dust concentration at different distances from the head (Fig. 19), it can be seen that under the condition of forced ventilation, dust in the roadway has unilateral accumulation, and the dust concentration in the position far from the air duct is relatively high. The reason may be that the tunneling machine and other equipment in the roadway have the blocking effect, which will block the airflow and change its direction. The airflow on the right side of the boring machine (away from the air duct side) produces higher speed and lower pressure, so that dust particles are more likely to accumulate on this side. In addition, the properties of dust particles also affect their behavior in the air flow. Particles with different characteristics will experience different forces in the air flow, resulting in unilateral aggregation. Dust diffusion has self-settling phenomenon. The dust concentration at the lower end is higher than that at the upper end and gradually diffuses pollution to the upper end. The reason is that dust particles themselves will move downward under the influence of gravity (Chen et al. 2022).

According to the change of dust concentration at the height of human breathing belt (Fig. 20), the dust concentration gradually decreases from the head to the back end of the roadway. The dust concentration is relatively high at the position of the tunneling machine, indicating that the arrangement and location of equipment and tools in the roadway can have an interception effect on the diffusion and propagation of dust particles. Therefore, a partition or barrier is set up in the roadway to block the airflow and the propagation of particulate matter. These obstructions can change the direction and speed of the air stream and cause particulate matter to accumulate or settle in the area behind them. In addition, Fig. 20 also shows that unilateral aggregation usually occurs on the side far from the air duct (air source). When the air duct or air source discharges air in a certain direction, dust particles are deflected in the air due to the difference in the flow direction and speed of the air duct. Driven by the air flow, dust particles move along the direction of the air flow in the return flow area, and the air flow forms a higher speed and lower pressure area near it, which leads to the accumulation of dust concentration in this area, and also forms the phenomenon of unilateral accumulation of dust under the pressurized ventilation condition. From the above analysis, it can be seen that, without considering other factors, the position of the tunneling machine driver near the side of the pressure air duct is less harmful to dust. In addition, the diffusion and propagation of dust particles

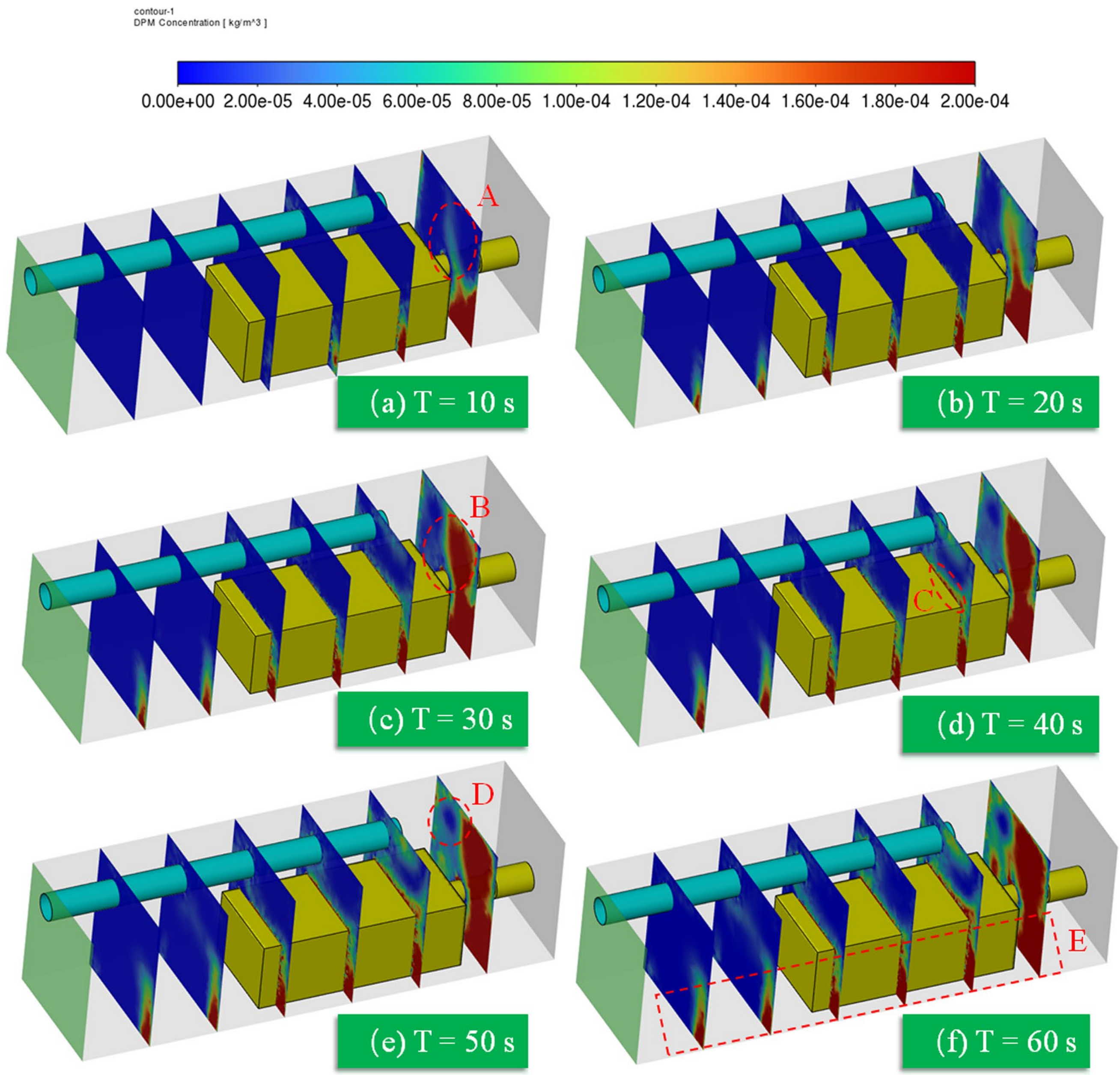

Fig. 19 Dust mass concentration at different distances from the heading face. **a** $T=10$ s **b** $T=20$ s **c** $T=30$ s **d** $T=40$ s **e** $T=50$ s **f** $T=60$ s

can be effectively prevented by the reasonable arrangement of obstacles in the roadway.

3.3 Discussion

The experimental and numerical simulation results show that the air flow field in the press-in ventilation roadway can be divided into three areas: jet zone, vortex zone and reflux zone, which is similar to the result in reference (Xiu et al. 2020). However, the formation of jet zone, vortex zone, and return zone requires a certain time, which can provide a theoretical basis for the installation position and opening time of the attached wall cyclone ventilation device on the mine duct or the air curtain device on the roadheader. The dust mass concentration on the side away from the air duct is significantly higher than that on the other side, which is similar to the conclusion in reference (Yao et al. 2020). Therefore, a dust removal device can be added on the return side of the roadway, especially near the roadheader with large dust collection volume, to reduce the dust concentration (Sun et al. 2019). There are two eddies at the front end of the heading machine, so targeted dust removal measures can be implemented for the eddies area. Spraying should be added at the entrance

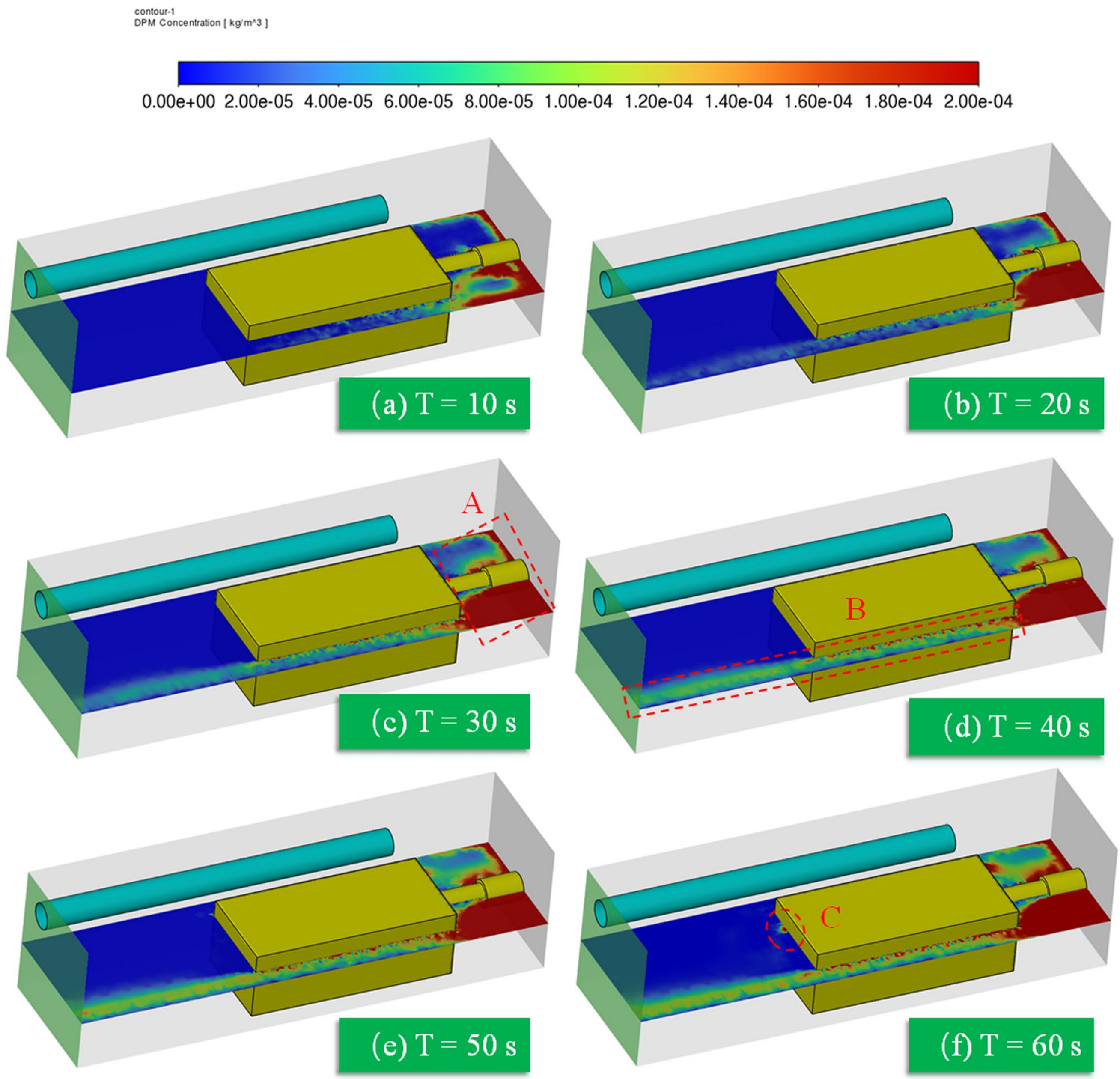

Fig. 20 Dust mass concentration at the height of breathing zone. **a** $T=10$ s **b** $T=20$ s **c** $T=30$ s **d** $T=40$ s **e** $T=50$ s **f** $T=60$ s

side to effectively capture small particles of dust (Zhang et al. 2020). This study helps to improve the understanding of dust distribution in the roadheading face and provides guidance for designing ventilation schemes and zoning to manage dust. On the other hand, this study can provide theoretical guidance for the determination of the optimal air velocity in the roadway and the optimal distance from the pressure duct to the face of the roadheading, and too high an increase in the air velocity does not necessarily lead to a decrease in the dust concentration all the time (Zheng et al. 2023a). However, this paper only investigated the distribution of dust in the roadway under forced ventilation conditions, which is useful for improving dust management in mines using this ventilation method. The experimental results may be different if a different ventilation method is used, such as the long-pressure, short-extraction ventilation method. Future research should focus on the development of new ventilation methods, such as the development of smart ducts and new wind control devices.

4 Conclusions

In this paper, experiments and numerical simulation are used to study the effects of wind speed and distance from the outlet to the driving face on dust diffusion and propagation. Finally, the following conclusions are drawn:

(1) The similarity criterion number of press-in ventilation dust removal model was deduced by similarity criterion. In order to ensure that the experiment is consistent with the site, the geometric similarity ratio of the experiment is 1: 2, a large pressure ventilation dust removal experimental model is built, and the relevant research on pressure ventilation dust removal is carried out through the similar experiment and numerical simulation. The research results can provide theoretical guidance for the application of the dust removal technology on the integrated mining face of coal mine.
(2) According to similar experimental results, there are optimal values for wind speed and distance from outlet to head. When the wind speed is 2 m/s and the distance from the outlet to the driving face is 1.8 m, the mass concentration of dust in the roadway is the minimum. The maximum error between the test value and the simulation model is 12.9%, which verifies the correctness of the experimental results.
(3) According to the numerical simulation results, the airflow field in the roadway with or without dust disturbance can be divided into three areas: jet zone, vortex zone and reflux zone. Dust concentration gradually decreases from the head to the back end of the roadway. Under the pressure ventilation condition, dust accumulates in one side, and the dust concentration is higher in the position far from the air duct. The arrangement and location of the equipment will have an interception effect on dust particles. Reasonable arrangement of obstacles can effectively prevent the diffusion and propagation of dust particles.

Acknowledgements This work was financially supported by the National Key R&D Program of China (2022YFC2503200, 2022YFC2503201), the National Natural Science Foundation of China (52074012, 52204191), the Anhui Provincial Natural Science Foundation (2308085J19), the University Distinguished Youth Foundation of Anhui Province (2022AH020057), the Anhui Province University Discipline (Major) Top Talent Academic Support Project (gxbjZD2022017), the Funding for academic research activities of reserve candidates for academic and technological leaders in Anhui Province (2022H301), the Independent Research fund of Key Laboratory of Industrial Dust Prevention and Control & Occupational Health and Safety, Ministry of Education (Anhui University of Science and Technology) (EK20211004), the Graduate Innovation Fund of Anhui University of Science and Technology (2023CX1003).

Author contributions HZ Data analysis, Drafted the manuscript. BJ Funding acquisition. HW Writing—review & editing. YZ Methodology.

Declarations

Competing interests The authors declare that they have no known competing financial interests or personal relationships that could have appeared to influence the work reported in this paper.

References

Ashish KR, Neeraj G, Steven S (2022) CFD modeling and laboratory studies of dust cleaning efficacy of an efficient four stage non-clogging impingement filter for flooded-bed dust scrubbers. Int J Coal Sci Technol 9(1):16. https://doi.org/10.1007/s40789-022-00481-5

Chen J (2018) Property experiments on the foam generator and its influencing factors during down-the-hole drilling. Process Saf Environ Prot 114:169–178

Chen L, Ma Y, Ghaleb M, Liu G (2022) Study on dust pollution law and ventilation optimization of roadway excavation and shotcrete simultaneous operation. J Clean Prod 379:134744

Chhabra RP, Gurappa B (2019) Coulson and Richardson's chemical engineering: Volume 2A: particulate systems and particle technology. Butterworth-Heinemann 44:215–218

Geng F, Luo G, Zhou F, Zhao P, Ma L, Chai H, Zhang T (2017) Numerical investigation of dust dispersion in a coal roadway with hybrid ventilation system. Powder Technol 313:260–271

Han H, Hetang W, Zhang Qi Du, Yunhe WH, Hui W (2023) Investigations of the effects of two typical jet crushing methods on the atomization and dust reduction performance of nozzles. Int J Coal Sci Technol 10(1):50. https://doi.org/10.1007/s40789-023-00606-4

Hou C, Yu H, Yang X, Cheng W, Wang Y, Ye Y (2022) Research on dust removal technology of large eddy dust collecting and swirl airflow distribution in the fully-mechanized excavation face. Powder Technol 411:117922

Hua Y, Nie W, Cai P, Liu Y, Peng H, Liu Q (2018) Pattern characterization concerning spatial and temporal evolution of dust pollution associated with two typical ventilation methods at fully mechanized excavation faces in rock tunnels. Powder Technol 334:117–131

Ji B, Jiang B, Yuan L, Yu C, Zhou G, Zhao Y, Wang S, Wang X (2023) Experimental and molecular dynamics simulation study on the influence of SDS and JFC composite ratios on bituminous coal wettability. Process Saf Environ Prot 174:473–484

Jiang B, Huang J, Yu C-F, Wang X-H, Zhou Y, Zheng Y, Ji B, Zhang Q (2023) Experimental and theoretical study on molecular structure construction of Hongliulin coal. Fuel 349:128708

Jin H, Zhang Y, Wu G, Yang J, Li N (2022) Optimization via response surface methodology of the synthesis of a dust suppressant and its performance characterization for use in open cut coal mines. J Environ Sci 121:211–223

Kollipara VK (2015) Development of dust aerosol control concepts through experimental and numerical techniques. Southern Illinois University at Carbondale 33:215–218

Kurnia JC, Sasmito AP, Mujumdar AS (2014) Dust dispersion and management in underground mining faces. Int J Min Sci Technol 24:39–44

Liu Q, Nie W, Hua Y, Peng H, Ma H, Yin S, Guo L (2019) Long-duct forced and short-duct exhaust ventilation system in tunnels: Formation and dust control analysis of pressure ventilation air curtain. Process Saf Environ Prot 132:367–377

Moreno T, Trechera P, Querol X, Lah R, Johnson D, Wrana A, Williamson B (2019) Trace element fractionation between PM10 and PM2.5 in coal mine dust: Implications for occupational respiratory health. Int J Coal Geol 203:52–59

Nie W, Wei W, Ma X, Liu Y, Peng H, Liu Q (2017) The effects of ventilation parameters on the migration behaviors of head-on dusts in the heading face. Tunn Undergr Space Technol 70:400–408

Nie W, Cai X, Peng H, Ma Q, Liu Q, Hua Y, Guo L, Cheng L, Sun N, Bao Q (2022a) Distribution characteristics of an airflow–dust mixture and quantitative analysis of the dust absorption effect during tunnel sub-regional coal cutting. Process Saf Environ Prot 164:319–334

Nie W, Sun N, Liu Q, Guo L, Xue Q, Liu C, Niu W (2022b) Comparative study of dust pollution and air quality of tunnelling anchor integrated machine working face with different ventilation. Tunn Undergr Space Technol 122:104377

Peng H, Nie W, Zhang X, Xu C, Meng X, Cheng W, Liu Q, Hua Y (2022) Research on the blowing-spraying synergistic dust removal technology for clean environment in large-scale mechanization coal mine. Fuel 324:124508

Sun B, Cheng W, Wang J, Wang H, Ma Y (2019) Development of Venturi negative-pressure secondary dedust device and application of local spray closure technique. Adv Powder Technol 30:42–54

Toraño J, Torno S, Menéndez M, Gent M (2011) Auxiliary ventilation in mining roadways driven with roadheaders: Validated CFD modelling of dust behaviour. Tunn Undergr Space Technol 26:201–210

Wang L, Lu Z, Chen D-P, Liu Q-Q, Chu P, Shu L-Y, Ullah B, Wen Z-J (2020) Safe strategy for coal and gas outburst prevention in deep-and-thick coal seams using a soft rock protective layer mining. Saf Sci 129:104800

Wang X-H, Jiang B, Yuan L, Zhao Y, Yu C-F, Zheng Y, Huang J, Ji B (2023) Study on coupling chelating agent and surfactant to enhance coal wettability: experimental and theoretical discussion. Fuel 342:127861

Xiong W, Fu L, Zhao G, Chen Y, Zhao X, Hu M, Yao H (2021) A new dust removal technology used in hot rolling mills: Atomized spray with higher dedusting efficiency. J Clean Prod 311:127574

Xiu Z, Nie W, Yan J, Chen D, Cai P, Liu Q, Du T, Yang B (2020) Numerical simulation study on dust pollution characteristics and optimal dust control air flow rates during coal mine production. J Clean Prod 248:119197

Yao H, Wang H, Li Y, Jin L (2020) Three-dimensional spatial and temporal distributions of dust in roadway tunneling. Int J Coal Sci Technol 7:88–96

Yin S, Nie W, Guo L, Liu Q, Hua Y, Cai X, Cheng L, Yang B, Zhou W (2020) CFD simulations of air curtain dust removal effect by ventilation parameters during tunneling. Adv Powder Technol 31:2456–2468

Yu H, Cheng W, Wu L, Wang H, Xie Y (2017) Mechanisms of dust diffuse pollution under forced-exhaust ventilation in fully-mechanized excavation faces by CFD-DEM. Powder Technol 317:31–47

Yu C-F, Jiang B, Yuan L, Zhang Y, Ji B, Zheng Y, Ren B (2023) Inhibiting effect investigation of ammonium dihydrogen phosphate on oxidative pyrolysis characteristics of bituminous coal. Fuel 333:126352

Zhang G, Zhou G, Zhang L, Sun B, Wang N, Yang H, Liu W (2020) Numerical simulation and engineering application of multistage atomization dustfall at a fully mechanized excavation face. Tunn Undergr Space Technol 104:103540

Zhang F, Lu Y, Wang Y, Cheng J, Jiang Z, Chen Y, Chen J (2022a) Study on air curtain cooperative spray dust removal in heading face based on swirl theory. J Environ Chem Eng 10:108892

Zhang Q, Xing X, Zhou G, Hu Y, Shang S, Fu M, Ma H, Li H, Men Y (2022b) Preparation and micro-wetting mechanism analysis of highly permeable-moistening additive for coal seam water injection based on plant extraction technology. Fuel 322:124125

Zhang Y, Zheng Y, Jiang B, Yu G, Ren B, Yu C, Wang S (2023) Experimental study on the influence of acid fracturing fluid on coal wettability. Fuel 343:127965

Zheng H, Jiang B, Zheng Y, Zhao Y, Wang H (2023a) Experimental study on forced ventilation and dust -control in a heading face based on response surface method. Process Saf Environ Prot 175:753–763

Zheng H, Shi S, Jiang B, Zheng Y, Li S, Wang H (2023) Research on coal dust wettability identification based on GA–BP model. Int J Environ Res Public Health. https://doi.org/10.3390/ijerph20010624

Zhou G, Zhang Q, Hu Y, Gao D, Wang S, Sun B (2020) Dust removal effect of negatively-pressured spraying collector for advancing support in fully mechanized coal mining face: Numerical simulation and engineering application. Tunn Undergr Space Technol 95:103149

Zhou G, Wang C, Liu R, Li S, Zhang Q, Liu Z, Yang W (2022) Synthesis and characterization of water injection fracturing fluid for wetting and softening coal seam. Int J Rock Mech Min Sci 150:105024

Zhou G, Jing B, Meng Q, Liu Y, Yang W, Sun B (2023) Study on coupling diffusion of composite dust and cloud-mist dedust technology in fully mechanized driving face of mixed coal-rock roadway. Adv Powder Technol 34:103911

Zhu JT, Chen ML, Wang L, Sun HS, Wang CH, Azhar N, Oduro NB (2023) Characterization of 10 nm – 10 μm coal dust particles generated by simulated different cutting and drilling parameters: mass concentration distribution, number concentration distribution, and fractal dimension. Int J Coal Sci Technol 10(1):89. https://doi.org/10.1007/s40789-023-00632-2